

HyperKAN: Kolmogorov-Arnold Networks make Hyperspectral Image Classifiers Smarter

Valeriy Lobanov ^{1,2}, Nikita Firsov ¹, Evgeny Myasnikov ¹, Roman Khabibullin ¹ and Artem Nikonorov ¹

¹ Samara National Research University, Samara, Russia;
² Adyge State University, Maykop, Republic of Adygea, Russia;
* Correspondence: firsov.na98@gmail.com;

Abstract: In traditional neural network architectures, a multilayer perceptron (MLP) is typically employed as a classification block following the feature extraction stage. However, the Kolmogorov-Arnold Network (KAN) presents a promising alternative to MLP, offering the potential to enhance prediction accuracy. In this paper, we propose the replacement of linear and convolutional layers of traditional networks with KAN-based counterparts. These modifications allowed us to significantly increase the per-pixel classification accuracy for hyperspectral remote-sensing images. We modified seven different neural network architectures for hyperspectral image classification and observed a substantial improvement in the classification accuracy across all the networks. The architectures considered in the paper include baseline MLP, state-of-the-art 1D (1DCNN) and 3D convolutional (two different 3DCNN, NM3DCNN), and transformer (SSFTT) architectures, as well as newly proposed M1DCNN. The greatest effect was achieved for convolutional networks working exclusively on spectral data, and the best classification quality was achieved using a KAN-based transformer architecture. All the experiments were conducted using seven openly available hyperspectral datasets. Our code is available at <https://github.com/f-neumann77/HyperKAN>.

Keywords: Kolmogorov-Arnold Networks; Hyperspectral Imaging; Classification; Transformers; Convolutional Neural Networks

1. Introduction

A hyperspectral image (HSI) is a three-dimensional structure with two spatial and one spectral coordinates. Unlike RGB and multispectral images, hyperspectral images are recorded at a much higher spectral resolution. Each material, which has a unique spectral signature that serves as a “fingerprint,” can be uniquely identified in a hyperspectral image [1, 2]. This allows one to perform analysis tasks such as classification of objects on HSI, segmentation, clustering, object detection, tracking changes in time series, etc., with higher quality compared to conventional RGB or multispectral images.

The most important task of HSI analysis is the task of pixelwise classification, which involves assigning class labels to image pixels based on their spectral characteristics. This kind of task is widely in demand in remote sensing, particularly for agricultural problems [3], environmental monitoring [4], cartography [5] (for example, determining the boundaries of reservoirs [5] and glaciers [6]), etc.

Since HSIs contain both spatial and detailed spectral information about the captured scene, analysis, in particular the classification of such images, requires the use of special tools [7]. To solve problems of HSI analysis, classical methods were used, namely the Spectral Angle Mapper (SAM) [8], spectral indices (NDVI, NDWI, etc.) [9] and others. In addition, general-purpose machine learning methods were utilized, such as SVM [10], decision trees [11], random forest [12], etc. However, such methods do not take into account spatial information contained in the HSI, and, moreover, cannot extract deeper dependencies in spectral data.

To extract deep features from spectral data more efficiently, deep architectures have been used. These architectures were based on convolutional neural networks, namely 1D networks [13], as well as based on the increasingly popular transformer architectures (see, for example, [14]).

To take into account spatial information, it is necessary to use deep learning tools based on spatial or spatial-spectral feature extractors. Such extractors were built based on two-dimensional convolutional layers (see, for example, 2D networks [15]) or three-dimensional convolutional layers (see 3D networks [16]). This allows a significant increase in classification quality in some cases compared to approaches that use exclusively spectral data.

Unfortunately, deep neural networks require huge amounts of data to train. HSI labeling is very labor-intensive, as it is often associated with ground-based measurements, which imposes restrictions on the use of deep neural networks for HSI analysis. For this reason, the ability of a neural network to learn from a small amount of data is an important aspect.

The deep learning algorithms is rapidly evolving, with significant advancements being made in new architecture designs. One example is networks based on the Kolmogorov-Arnold theorem [17], which have shown high efficiency in deep learning tasks. Such networks are called Kolmogorov-Arnold networks (KAN).

For example, in the paper [18] authors show that KANs outperform conventional Multi-Layer Perceptrons (MLPs) in a real-world satellite traffic forecasting task, providing more accurate results with considerably fewer learnable parameters. In the article [19], the authors show that KAN offers a promising alternative for efficient image analysis in the remote sensing field. In the paper [20], the authors show that KAN significantly outperforms MLP in terms of accuracy and convergence speed for numerous partial differential equations in computational solid mechanics, except for the complex geometry problem. In the paper [21] preliminary results indicate that while KANs are on par with MLPs in classification tasks, they seem to have a clear advantage in the graph regression tasks.

The purpose of this paper is to demonstrate the feasibility of replacing classical layers with their KAN analogs to improve the quality of HSI classification. This paper makes the following contributions:

- We take seven neural network architectures (MLP, 1DCNN [22], M1DCNN, 3DCNN [23], 3DCNN [24], NM3DCNN [25], SSFTT [26]) for HSI classification and transform them using KAN blocks, thus obtaining seven corresponding KAN-based architectures;
- Using seven different open HSI datasets we prove the advantage of each of seven KAN-based architectures over their classical counterparts, solving the problem of pixelwise HSI classification;
- We propose the M1DCNN architecture, which is a modification of the 1DCNN network. M1DCNN features an additional convolutional layer and a BatchNorm1D layer, which improves performance.

We describe the contributions in detail below. In Section 2, we briefly describe the replaceable blocks of classical neural networks and their KAN analogs. Next, we consider five different neural network architectures, as well as two modifications, including M1DCNN. In the same section, we show how these architectures can be transformed using KAN blocks and propose corresponding KAN-based architectures. In the third section, we briefly describe seven hyperspectral datasets used in the study, as well as the experimental conditions. Next, we show the results of a study for all the neural networks considered in Section 2 and discuss the experimental results in detail. The work ends with a conclusion and a list of references.

2. Materials and Methods

Typical neural network architectures for hyperspectral image classification can be described by a two-block scheme consisting of:

- Deep feature extractor;
- Classifying block (based on MLP or single linear layer).

In contrast to MLPs, which have fixed activation functions on nodes (neurons), KANs have learnable activation functions on edges (weights). KANs do not use linear weights; instead, each weight parameter is replaced by a one-dimensional function parameterized as a spline. This approach allows KAN to achieve better accuracy and interpretability compared to MLP [17]. Also utilizing KAN in traditional architectures such as U-Net [27] leads to improved quality indicators.

In this paper, we modify both the classifying block and the feature extraction block through the use of KAN-based layers. The study focused on several architectures including simple MLP, one-dimensional and three-dimensional convolutional architectures, and a transformer. We believe that these modifications will improve the classification quality indicators.

2.1. KAN blocks

Let's look at how modifications were made. The classifying block was modified to include KAN with two hidden layers instead of the original configuration. We will refer to this block as the Linear-KAN Block [17]. Similarly, the linear layers in an attention mechanism or convolutional layers in the feature extractor block may need to be replaced with KAN analogs.

3.1.1. Linear-KAN Block

The Linear-KAN Block is designed to replace the classification block in traditional neural network architectures. The architecture of the block consists of two hidden layers of size 512, followed by the Batch Norm1D layer.

We utilized the code of the block from the Efficient KAN project [28], which speeds up the original pyKAN implementation [29].

2.1. Conv2D-KAN Block

The Conv2D-KAN block is designed to replace the two-dimensional convolutional layer in the feature extractor of traditional neural network architectures. The idea is to replace linear multiplication operations with their KAN counterparts [30].

We used the implementation from the KA-Conv project [31], and implemented additional nonlinearities, namely, Radial Basis Function, Fourier Basis Function, Polynomial Function, Chebyshev Function, BSpline Function.

2.2. Architectures

To demonstrate the effectiveness of the KAN blocks described above, we selected the following neural network architectures utilized in literature for HSI classification:

- MLP;
- 1DCNN [22] and its modification M1DCNN proposed in this paper;
- 3DCNN [23];
- 3DCNN [24] and its modification NM3DCNN [25];
- SSFTT [26].

In each of these architectures, we replaced the classification layers with the Linear-KAN Block. Also, we optionally replaced the layers in the Attention mechanism with the Linear-KAN blocks and two-dimensional convolutional layers with the Conv2D-KAN blocks. For the Linear-KAN blocks, we utilized ReLU as an activation function. For the Conv2D-KAN blocks, we selected the activation function experimentally. The remaining KAN parameters were adopted from the original implementation [28] as follows:

- Grid size = 5;
- Spline order = 3;
- Scale noise = 0.1;
- Scale base = 1.0;
- Scale spline = 1.0;
- Grid eps = 0.02;
- Grid range = [-1, 1]).

2.2.1. MLP KAN

Since MLP remains relevant and is employed in various modifications in HSI classification [32- 34], we took it as a baseline architecture. In particular, we implemented a classic multilayer perceptron containing two hidden layers of 512 neurons in each layer. As an alternative to MLP, we also used a Linear-KAN block with the same number of parameters.

2.2.2. 1DCNN

The 1DCNN architecture was proposed by Wei Hu and others in their paper [22] in 2015. The main concept of the paper involves using one-dimensional convolutional layers to extract deep spectral features, followed by the use of MLP to address the problem of HSI classification. The architecture comprises a one-dimensional convolutional layer, a Max Pooling layer, and two fully connected layers (refer to Figure 1a). It is worth noting that this neural network operates exclusively with spectral data and does not use spatial relationships.

The proposed modification (hereinafter referred to as 1DCNN KAN) to the 1DCNN architecture described above involves replacing the classifying block, which consists of hidden and classifying fully connected layers, with a Linear-KAN block. The Linear-KAN block has similar input and output dimensions, and consists of two hidden layers of size 512, followed by the Batch Norm1D layer (refer to Figure 1b). We used ReLU as a base nonlinear function in the Linear-KAN block.

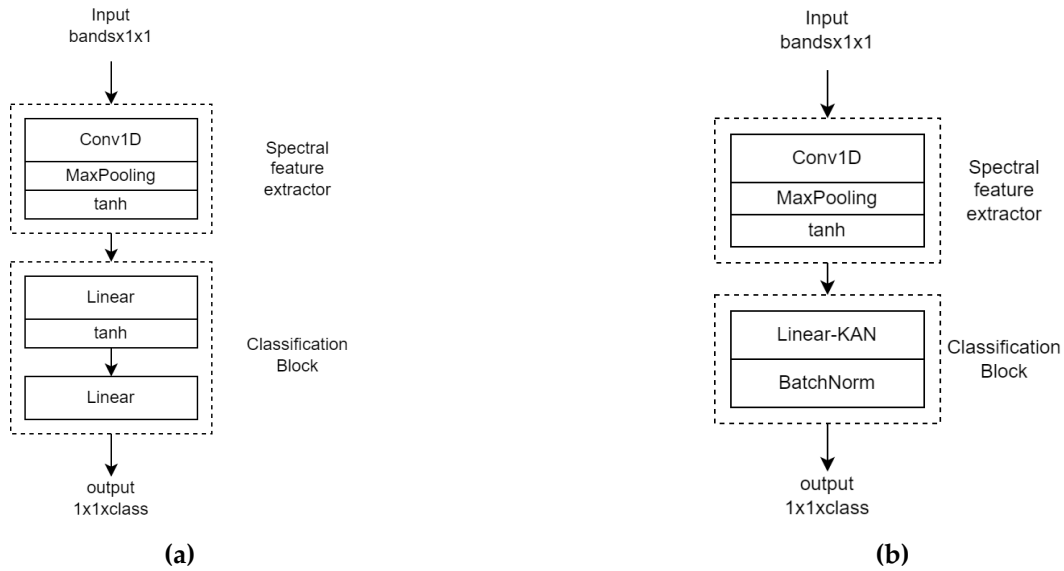


Figure 1. The architecture of 1DCNN (a) and the proposed modification 1DCNN KAN (b).

2.2.3. M1DCNN

In our paper, we introduce a modification to the 1DCNN architecture. We aim to enhance the feature extractor block by incorporating an extra convolutional layer and a Batch Norm 1D layer (refer to Figure 2a). This enhancement expands the feature extractor's capabilities while working solely with spectral features. Hereinafter we will refer to the described modification as M1DCNN.

Additionally, we revised the proposed M1DCNN architecture by substituting fully connected layers (both hidden and classifying) with the Linear-KAN block. This block has similar input and output dimensions and consists of two hidden layers of size 512, along with a Batch Norm 1D layer (refer to Figure 2b). Just like before, ReLU was used as the base nonlinear function. We will refer to this latter modification as M1DCNN KAN.

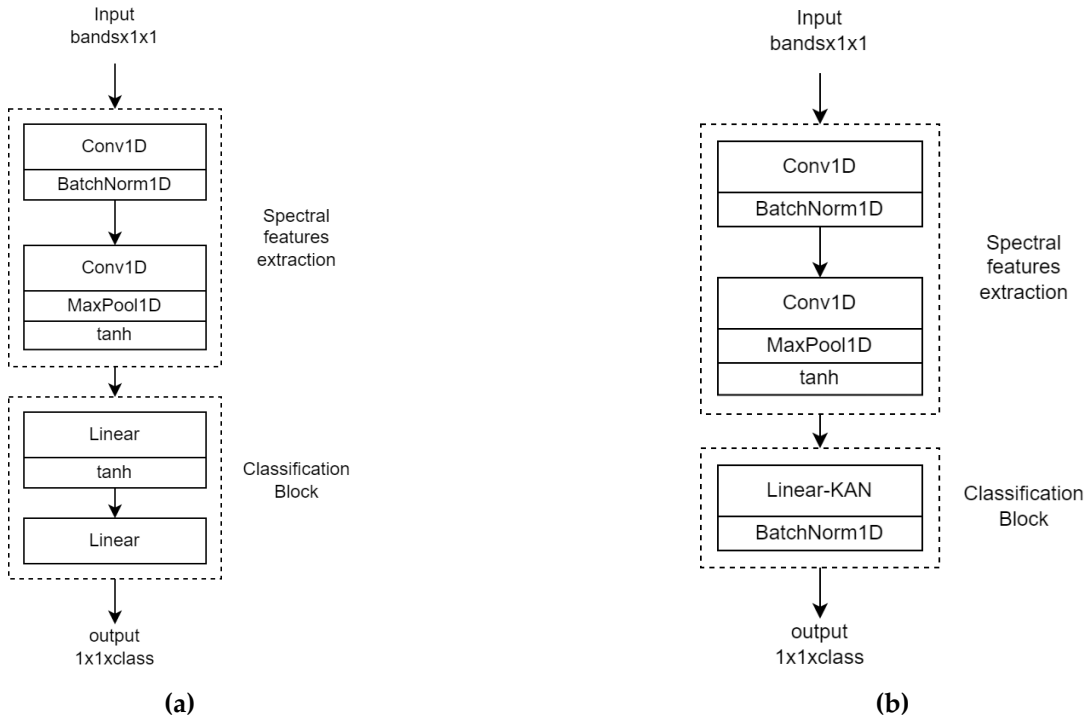


Figure 2. The proposed M1DCNN architecture (a) and its modification M1DCNN KAN (b).

2.2.4. 3DCNN by Luo

The 3DCNN architecture proposed by Yanan Luo and others in 2018 [23] combines 3D and 2D convolutional layers to extract deep spatial-spectral features. The architecture consists of an input 3D convolutional layer with a $24 \times 3 \times 3$ window, a two-dimensional convolutional layer with a 3×3 window, and two linear layers in a classifier (see Figure 3a).

In this paper, we propose to replace the two-dimensional convolution layer with its KAN analog with the nonlinear RBF function, as it delivered the best results in our experiments. In addition, we replaced the classification block as described above (see Figure 3b).

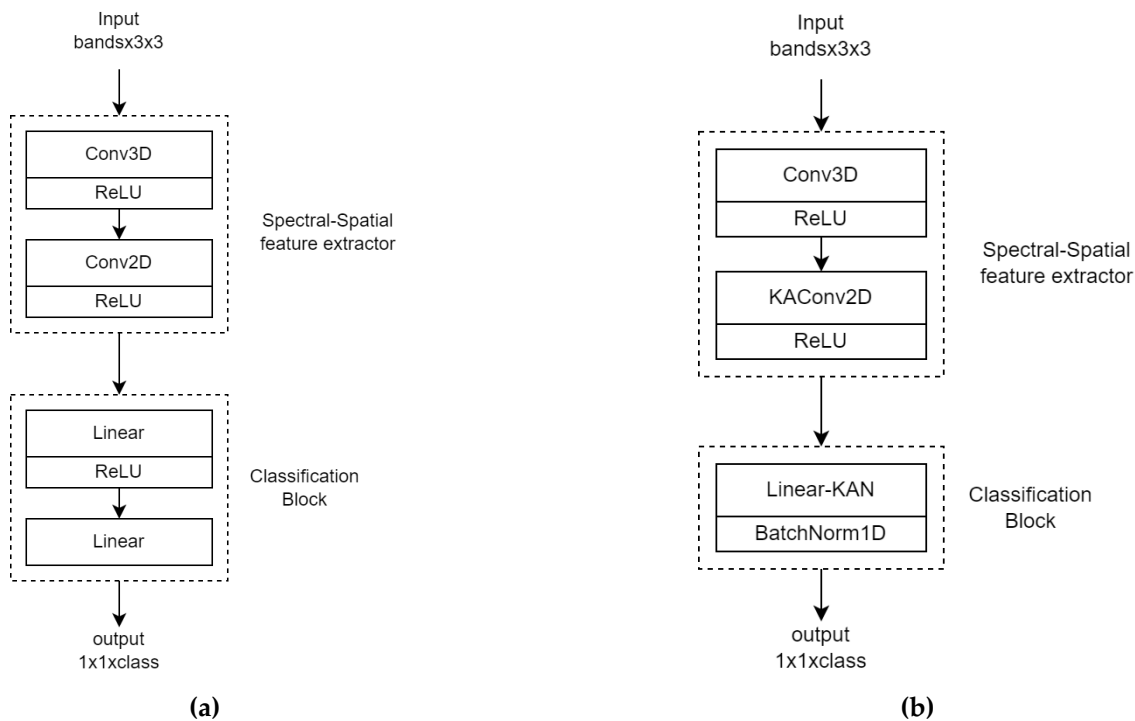


Figure 3. The architecture 3DCNN Luo (a) and the proposed modification 3DCNN Luo KAN (b).

2.2.5. 3DCNN by He

The 3DCNN He architecture was introduced by Mingyi He and others in their paper [24] in 2017. The main idea of the paper is the use of three-dimensional convolutions to extract spectral-spatial features and the utilization of blocks of parallel one-dimensional convolutions.

The architecture comprises a three-dimensional convolutional layer for extracting primary spectral-spatial features, subsequent two blocks of four parallel convolutional layers (ConvBlock) with different convolution kernel sizes to extract more diverse spectral-spatial features of the data (refer to Figure 4), another three-dimensional convolutional layer and a fully connected classifying layer (refer to Figure 5a).

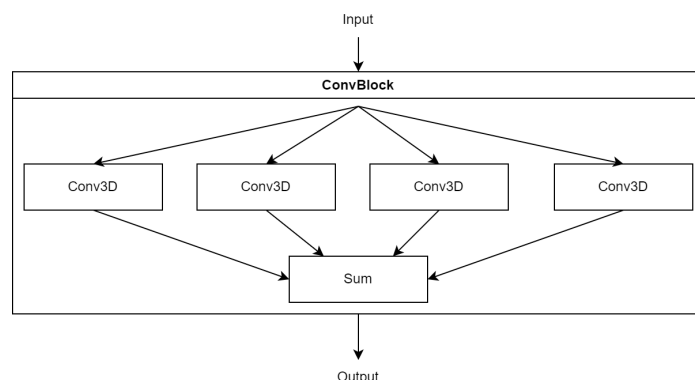


Figure 4. The architecture ConvBlock.

The proposed modification (hereinafter referred to as 3DCNN He KAN) of the 3DCNN He architecture (as shown in Figure 5b) involves replacing the fully connected classification layer with Linear-KAN block possessing similar input and output dimensions. This block contains two hidden layers of size 512, and the BatchNorm1D layer. The base nonlinear function used is ReLU.

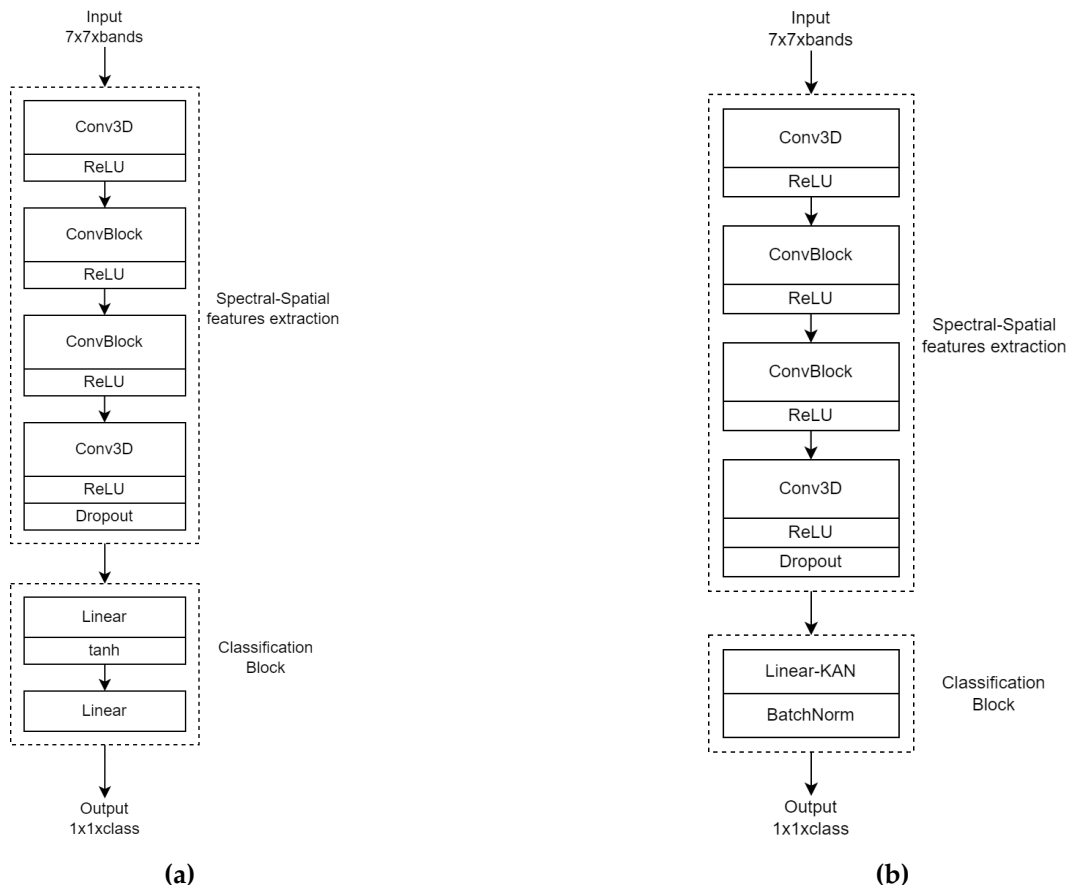


Figure 5. The architecture of 3DCNN He [24] (a) and the proposed modification 3DCNN He KAN (b).

2.2.6. NM3DCNN

The NM3DCNN architecture [25] introduced by Firsov N.A. and others in 2021 is a modification of the described earlier 3DCNN He architecture. The concept behind this modification (Figure 6 and Figure 7a) is to add BatchNorm layers after each convolutional layer to stabilize training and eliminate Dropout layer.

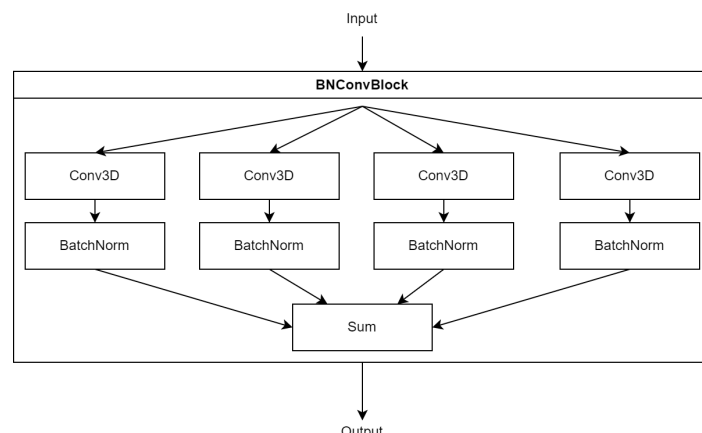


Figure 6. The architecture BNConvBlock.

The modification of the NM3DCNN architecture proposed in this paper (hereinafter referred to as NM3DCNN KAN) includes replacing the fully connected classification layer with the Linear-KAN block having the same input and output dimensions and consisting of two hidden layers of size 512, and the Batch Norm1D layer (see Figure 7b). ReLU was used as a base nonlinear function.

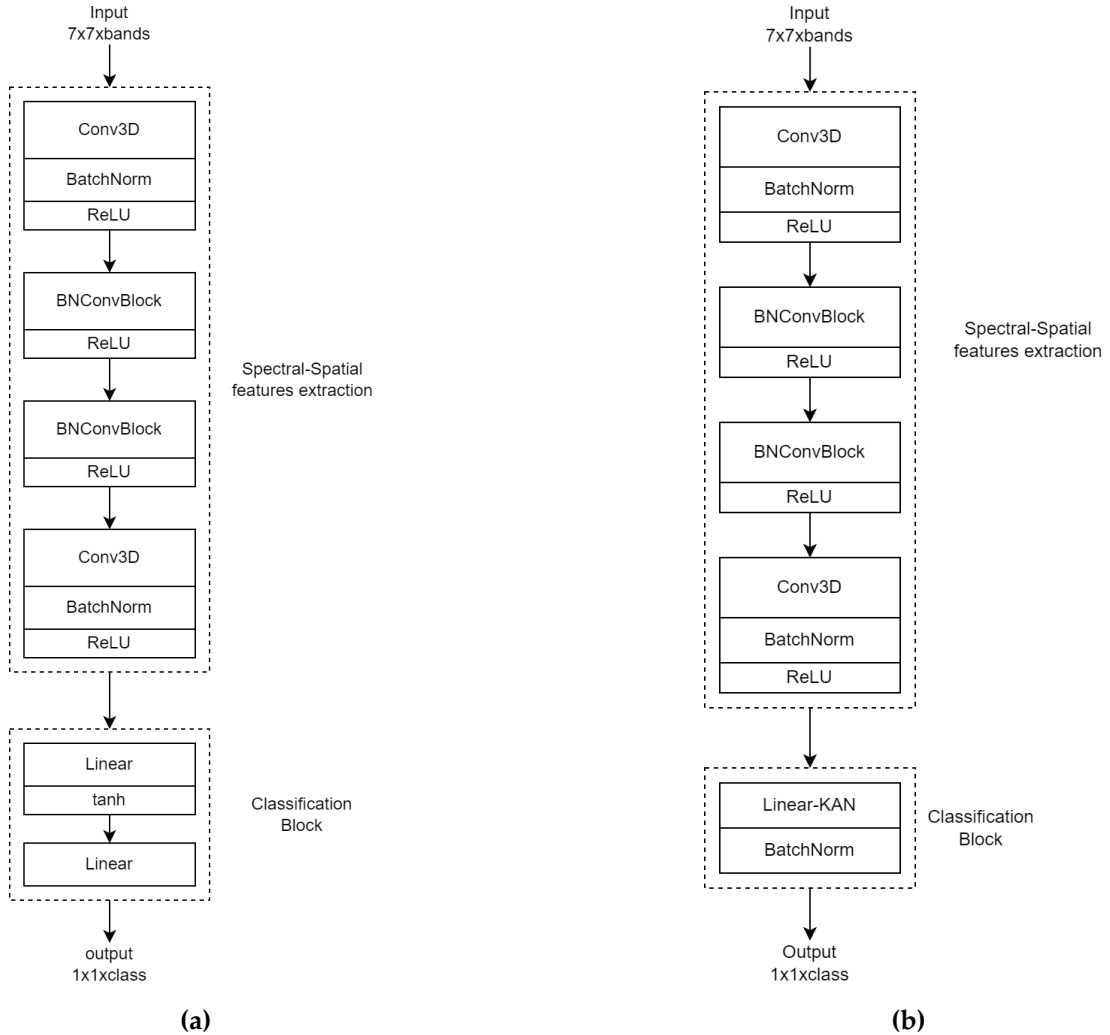


Figure 7. The architecture of NM3DCNN (a) and the proposed modification NM3DCNN KAN (b).

2.2.7. SSFTT

The SSFTT transformer architecture [26] proposed by Le Sun and others in 2022 is a combination of a spatial-spectral feature extractor, a tokenizer, a transformer encoder and a classifying linear layer. The advantage of this architecture is the use of convolutional layers to extract spatial-spectral features along with a trainable tokenizer equipped with an attention mechanism (refer to Figure 8a).

The proposed modification (hereinafter referred to as SSFTT KAN) of the SSFTT architecture includes the following changes only in the feature extraction block and the transformer block (Figure 8b):

- The replacement of two fully connected linear layers with a Linear-KAN block containing four hidden layers of size 512, maintaining the input and output dimensions of the MLP block taken from the KAN GPT implementation [35], as this implementation is intended for transformer architectures;
- The replacement of two fully connected layers within the Attention block with a Linear-KAN block consisting of four hidden layers of size 512, while preserving the input and output dimensions (taken from the KAN GPT implementation [35]);

- The replacement of the 2D-convolutional layer with a KA-Conv implementation of the KAN convolutional layer [31] with a 3x3 convolution kernel, maintaining the input and output dimensions. The RBF and Poly functions were used as base nonlinearities.

Replacing the classification block did not give us any increase in performance. Therefore, we left this block unchanged.

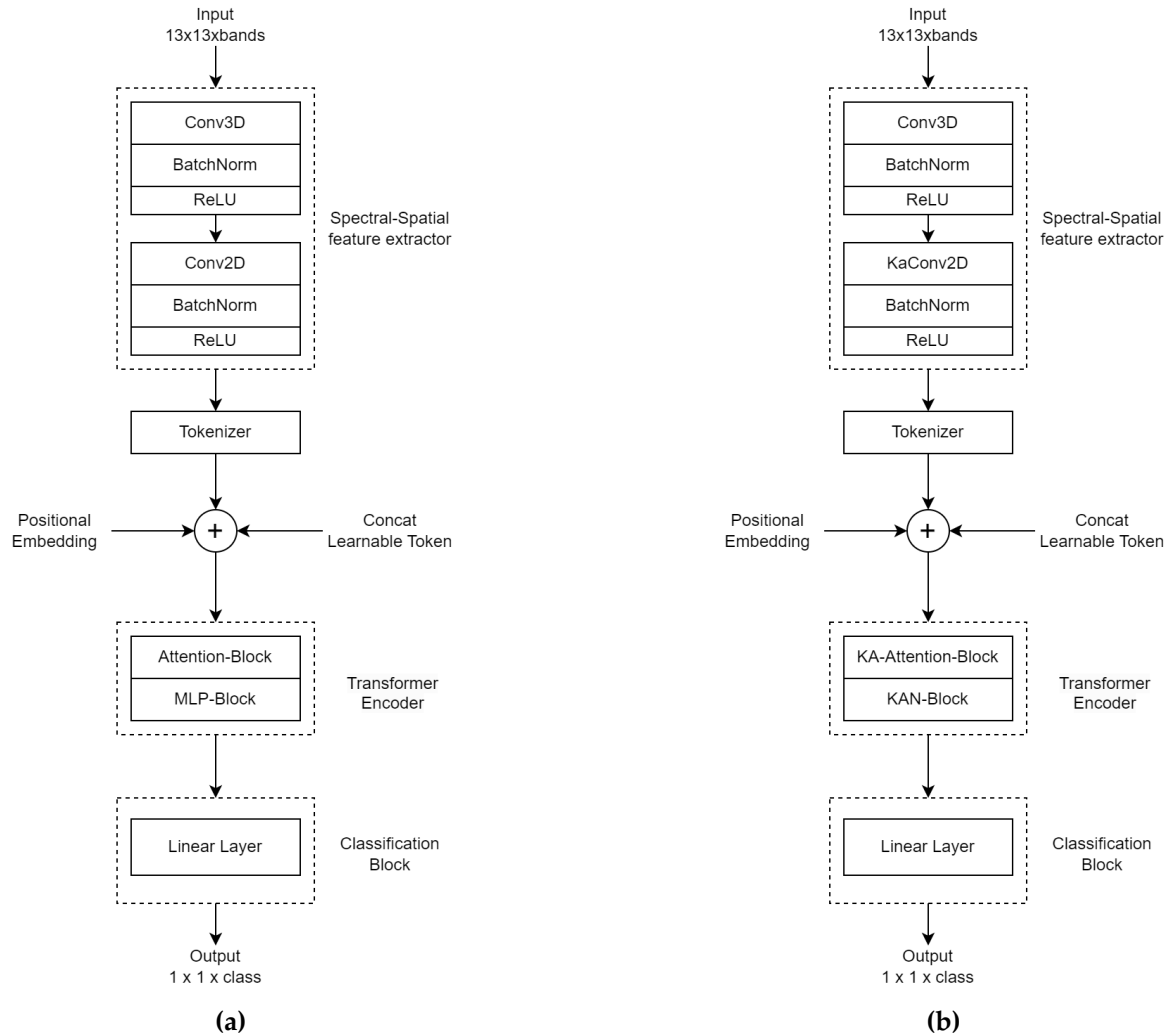


Figure 8. The SSFTT architecture **(a)** and the proposed modification of the SSFTT architecture **(b)**.

3. Results

3.1. Description of datasets

In our study, we used seven different open hyperspectral datasets listed in Table 1 along with their characteristics.

For the Pavia University and Indian Pines scenes, we chose 20% of random pixels from each class for the training set. For the remaining datasets (PaviaC, Salinas, Houston 13, Houston 18, and KSC) we chose 10% of random pixels from each class. Consequently, the test set consisted of 80% of the data for PaviaU and Indian Pines, and 90% for the other datasets. The strategy for choosing such a data partition was based on the search for the optimal architecture of a neural network classifier that could work on a small set of training data.

For the SSFTT architecture, the PCA technique was applied with the reduction to 30 components, as it was done in the original paper.

Table 1. Datasets.

Dataset Name	Size	Spectral channels	Number of classes	Classes
PaviaU	610x340	103	9	Void, Asphalt, Meadows, Gravel, Trees, Painted metal sheets, Bare soil, Bitumen, Self-blocking bricks, Shadows
PaviaC	1096x715	102	9	Void, Water, Trees, Meadows, Self-blocking bricks, Bare soil, Asphalt, Bitumen, Tiles, Shadows
Salinas	512x217	204	16	Void, Green weeds 1, Green weeds 2, Fallow, Fallow rough plow, Fallow smooth, Stubble, Celery, Grapes Untrained, Soil vinyard, Corn senesced, Luttuce romaine 4 wk, Luttuce romaine 5 wk, Luttuce romaine 6 wk, Luttuce romaine 7 wk, Vinyard_untrained, Vinyard_vertical
Indian Pines	145x145	200	16	Void, Alfalfa, Corn-notill, Corn-min, Corn, Grass/Pasture, Grass/Trees, Grass pasture/mowed, Hay-windrowed, Oats, Soybeans-no till, Soybeans-min till, Soybeans-clean till, Wheat, Woods, Buildings-grass-trees-Drive, Store-steel-towers
Houston 13	954x210	48	7	Void, Grass healthy, Grass stressed, Trees, Water, Residential Buildings, Non-residential Buildings, Road
Houston 18	954x210	48	7	Void, Grass healthy, Grass stressed, Trees, Water, Residential Buildings, Non-residential Buildings, Road
KSC	512x614	176	13	Void, Scrub, Willow swamp, CP hammock, Slash pine, Oak/Broadleaf, Hardwood, Swamp, Graminoid marsh, Spartina marsh, Cattail marsh, Salt marsh, Mud flats, Water

3.2. Experimental results

We considered MLP and KAN as baseline architectures, which exclusively process spectral features (pixels of hyperspectral images) and do not incorporate any spatial context.

Most of the original architectures considered in this study (1DCNN, M1DCNN, 3DCNN Luo, 3DCNN He, and NM3DCNN) were trained for 50 epochs with a learning rate of 0.2. The modified versions of these architectures (1DCNN KAN, M1DCNN KAN, 3DCNN Luo KAN, 3DCNN He KAN, and NM3DCNN KAN) were trained with a learning rate of 0.02 for improved convergence. Adam optimizer and StepLR scheduler (with parameters step_size=15 and gamma=0.5) were utilized for both original and modified architectures.

The SSFTT and SSFTT KAN networks were trained for 100 epochs, with learning rates of lr=0.01 and lr=0.008 for the original and modified architectures, respectively. Both networks utilized AdamW optimizer and StepLR scheduler with parameters step_size=20 and gamma=0.5. A batch size of 64 was used. In addition, for both architectures, the principal component analysis (PCA) technique was used to extract the first 30 principal components.

All the described models were trained from scratch.

The results of the experiments are presented in Tables 2 and 3.

We grouped the results for the specified architectures based on the window size used by the networks to extract spatial features. The architectures 1DCNN, 1DCNN KAN, M1DCNN, and M1DCNN KAN do not use spatial context, while 3DCNN Luo, 3DCNN Luo KAN utilize a 3x3 spatial window, 3DCNN He, 3DCNN He KAN, NM3DCNN and NM3DCNN KAN utilize a 7x7 spatial window. SSFTT and SSFTT KAN, stand apart, with the spatial patch sizes for these networks being 13x13.

In the last column, for each pair of original and KAN-based neural networks, we present the classification quality gain averaged over all used datasets.

Table 2. Overall classification accuracy (OA) for various neural network models and datasets, in percent.

Model Name	Dataset Name							Average gain
	PaviaU*	PaviaC	Salinas	Indian Pines*	Houston13	Houston 18	KSC	
Baseline approaches								
MLP	91.43	97.1	92.32	79.2	87.58	86.27	86.24	
KAN	94.12	98.25	93.25	84.0	94.19	87.20	88.10	2.71
Spectral features only								
1DCNN	92.9	97.4	92.0	83.7	92.1	86.7	79.1	
1DCNN KAN	95.6	99.1	94.6	90.2	96.5	90.6	89.3	4.5
M1DCNN	94.7	98.5	92.8	84.8	81.3	90.4	85.0	
M1DCNN KAN	95.3	99.1	95.2	89.2	97.4	93.2	90.4	4.6
Spectral-spatial features (window size 3x3)								
3DCNN Luo	96.09	98.40	93.30	83.01	94.50	91.79	87.52	
3DCNN Luo KAN	96.69	98.69	94.4	90.15	98.06	93.37	91.8	2.56
Spectral-spatial features (window size 7x7)								
3DCNN He	94.4	97.6	93.0	83.4	89.3	87.9	90.1	
3DCNN He KAN	95.5	98.3	94.4	88.2	90.9	90.8	91.6	2
NM3DCNN	94.3	98.2	93.0	85.4	91.3	89.9	91.2	
NM3DCNN KAN	95.8	98.7	96.2	90.7	96.6	91.9	94.4	3
Spectral-spatial features (window size 13x13), 30 principal components								
SSFTT	99.68	99.90	99.97	98.89	98.59	96.03	86.32	
SSFTT KAN	99.80	99.91	99.98	99.05	98.85	96.04	91.10	0.86

* The training sample size for PaviaU and Indian Pines consisted of 20% samples per class, while for other datasets it was 10% per class.

Table 3. Weighted F1 measure for various neural network models and datasets.

Model Name	Dataset Name							Average gain
	PaviaU*	PaviaC	Salinas	Indian Pines*	Houston13	Houston 18	KSC	
Baseline approaches								
MLP	0.914	0.971	0.922	0.784	0.871	0.867	0.857	
KAN	0.942	0.982	0.932	0.835	0.940	0.873	0.878	0.028
Spectral features only								
1DCNN	0.928	0.974	0.917	0.835	0.919	0.867	0.769	
1DCNN KAN	0.956	0.990	0.947	0.901	0.965	0.906	0.892	0.049
M1DCNN	0.946	0.985	0.928	0.872	0.807	0.904	0.834	
M1DCNN KAN	0.952	0.991	0.952	0.891	0.974	0.933	0.902	0.045
Spectral-spatial features (window size 3x3)								
3DCNN Luo	0.966	0.986	0.934	0.831	0.946	0.923	0.873	
3DCNN Luo KAN	0.972	0.988	0.945	0.903	0.982	0.940	0.921	0.027
Spectral-spatial features (window size 7x7)								
3DCNN He	0.960	0.981	0.940	0.839	0.898	0.894	0.903	
3DCNN He KAN	0.971	0.988	0.955	0.891	0.915	0.925	0.915	0.020
NM3DCNN	0.958	0.987	0.940	0.861	0.917	0.916	0.911	
NM3DCNN KAN	0.973	0.992	0.972	0.917	0.973	0.936	0.945	0.031
Spectral-spatial features (window size 13x13), 30 principal components								
SSFTT	0.9968	0.9990	0.9997	0.9889	0.9859	0.9603	0.8632	
SSFTT KAN	0.9980	0.9991	0.9998	0.9905	0.9885	0.9604	0.9110	0.0076

* The training sample size for PaviaU and Indian Pines consisted of 20% samples per class, while for other datasets it was 10% per class.

4. Discussion

All considered solutions provided a fairly high level of quality. Let's start the analysis with classical architectures. The basic MLP approach was the least effective in terms of the classification quality in over half of the cases (scenes PaviaU, PaviaC, Indian Pines, Houston 18), which was expected. Among convolutional networks with a classical architecture that use only spectral information (1DCNN, M1DCNN), the modified M1DCNN network proposed in this paper seems more advantageous, being inferior to the 1DCNN network only in one image (Houston13). Among the networks based on spectral-spatial convolutions (3DCNN Luo, 3DCNN He, NM3DCNN), we prefer the 3DCNN Luo, which, using a smaller spatial window size, outperformed the 3DCNN He and NM3DCNN networks on all the considered datasets, except the Indian Pines and KSC images. Given a choice between 3DCNN He and NM3DCNN, we would choose the latter, as it provided better quality compared to 3DCNN for all the scenes, except PaviaU. The results obtained by SSFTT are noticeably higher than for other classical neural networks considered. We suspect that the significantly larger spatial window (context) size is the main reason for this difference.

The primary objective of this study was not to compare different neural network architectures, but instead to highlight the advantages of KAN-based architectures over their traditional counterparts. Let's take a look at the results obtained by neural networks based on KAN blocks.

The results show that replacing linear and convolutional layers with KAN analogs is appropriate. An improvement in quality compared to traditional analogs was observed in all the considered cases. The greatest effect from the use of KAN was achieved for convolutional networks working exclusively on spectral data. We observe 0.6-16.1% increase in classification accuracy with an average increase of 4.5% and 4.6% for 1DCNN KAN and M1DCNN KAN, respectively. The average increase in classification accuracy for two convolutional 3DCNN KAN

and NM3DCNN KAN networks was 2-3%. Although the smallest increase in quality was observed for the transformer SSFTT KAN network (the average increase was less than 1%), this network achieved the best classification quality.

In our experiments, in most cases using Linear-KAN layers before MLP as the final classifying layer shows a significant increase in performance. However, implementing a KAN-based convolutional layer only leads to a small improvement in classification quality, particularly when using the Radial Basis Function and B-spline. In the case of the transformer architecture, replacing the classifying block did not significantly improve the classification accuracy. However, the replacement in the attention and MLP blocks allowed the modified transformer to increase the quality indicators. It is worth noting that using KAN layers resulted in better convergence, but training such networks takes a bit longer.

5. Conclusions

In this paper, we proposed to build analogues of traditional neural networks for HSI analysis using KAN. We modified seven different neural network architectures (including MLP, transformer SSFTT, convolutional 1DCNN, 3DCNN Luo, 3DCNN He, NM3DCNN, and M1DCNN proposed in this paper) and obtained a noticeable improvement in classification accuracy for all the considered networks.

The greatest effect from the use of KAN was achieved for 1DCNN KAN and M1DCNN KAN convolutional networks working exclusively on spectral data. The smallest increase in classification quality was observed for the transformer SSFTT KAN network, while this network showed the best classification quality. The average increase in classification accuracy for the spectral-spatial convolutional networks (3DCNN Luo KAN, 3DCNN He KAN and NM3DCNN KAN) was 2-3%.

We observed that for training networks equipped with KAN blocks, a reduction in learning rate (sometimes by an order of magnitude) is required relative to the classic architectures. It is worth noting that the implementation of Linear-KAN layers had a greater impact on the final quality of classification compared to KAN-based convolutional layers.

References

1. Lu, G.; Fei, B. Medical hyperspectral imaging: a review. *Journal of Biomedical Optics* **2014**, *19*(1), 010901. <https://doi.org/10.1117/1.JBO.19.1.010901>
2. Klein, M.E.; Aalderink, B.J.; Padoan, R.; de Bruin, G.; Steemers, T.A.G. Quantitative Hyperspectral Reflectance Imaging. *Sensors* **2008**, *8*, 5576-5618. <https://doi.org/10.3390/s8095576>
3. Wang, C.; Liu, B.; Liu, L. et al. A review of deep learning used in the hyperspectral image analysis for agriculture. *Artif Intell Rev* **2021**, *54*, 5205-5253. <https://doi.org/10.1007/s10462-021-10018-y>
4. Sun, G.; Jiao, Z.; Zhang, A.; Li, F.; Fu, H.; Li, Z. Hyperspectral image-based vegetation index (HSVI): A new vegetation index for urban ecological research. *International Journal of Applied Earth Observation and Geoinformation* **2021**, *103*, 102529. <https://doi.org/10.1016/j.jag.2021.102529>
5. Liu, C.; Tao, R.; Li, W.; Zhang, M.; Sun, W.; Du, Q. Joint Classification of Hyperspectral and Multispectral Images for Mapping Coastal Wetlands. *IEEE Journal of Selected Topics in Applied Earth Observations and Remote Sensing* **2020**, *99*, 1-15. <https://doi.org/10.1109/JSTARS.2020.3040305>
6. Sood, V.; Tiwari, R.K.; Singh, S.; Kaur, R.; Parida, B.R. Glacier Boundary Mapping Using Deep Learning Classification over Bara Shigri Glacier in Western Himalayas. *Sustainability* **2022**, *14*, 13485. <https://doi.org/10.3390/su142013485>
7. Nalepa, J. Recent Advances in Multi- and Hyperspectral Image Analysis. *Sensors* **2021**, *21*, 6002. <https://doi.org/10.3390/s21186002>
8. Chakravarty, S.; Paikaray, B.K.; Mishra R.; Dash, S. Hyperspectral Image Classification using Spectral Angle Mapper. *Proceedings of the IEEE International Women in Engineering (WIE) Conference on Electrical and Computer Engineering (WIECON-ECE)* **2021**, 87-90. <https://doi.org/10.1109/WIECON-ECE54711.2021.9829585>
9. Ju, Y.; Bohrer, G. Classification of Wetland Vegetation Based on NDVI Time Series from the HLS Dataset. *Remote Sens.* **2022**, *14*, 2107. <https://doi.org/10.3390/rs14092107>
10. Wang, Y.; Yu, W.; Fang, Z. Multiple Kernel-Based SVM Classification of Hyperspectral Images by Combining Spectral, Spatial, and Semantic Information. *Remote Sens.* **2020**, *12*, 120. <https://doi.org/10.3390/rs12010120>
11. Xu, S.; Liu, S.; Wang, H.; Chen, W.; Zhang, F.; Xiao, Z. A Hyperspectral Image Classification Approach Based on Feature Fusion and Multi-Layered Gradient Boosting Decision Trees. *Entropy* **2021**, *23*, 20. <https://doi.org/10.3390/e23010020>
12. Wang, Z.; Zhao, Z.; Yin, C. Fine Crop Classification Based on UAV Hyperspectral Images and Random Forest. *ISPRS Int. J. Geo-Inf.* **2022**, *11*, 252. <https://doi.org/10.3390/ijgi11040252>
13. Huang, J.; He, H.; Lv, R.; Zhang, G.; Zhou, Z.; Wang, X. Non-destructive detection and classification of textile fibres based on hyperspectral imaging and 1D-CNN. *Analytica Chimica Acta* **2022**, *1224*, 340238. <https://doi.org/10.1016/j.aca.2022.340238>

14. Hong, D.; Han, Z.; Yao, J.; Gao, L.; Plaza, A.; Chanussot, J. SpectralFormer: Rethinking Hyperspectral Image Classification With Transformers. *IEEE Transactions on Geoscience and Remote Sensing* **2021**, *60*, 5518615. <https://doi.org/10.1109/TGRS.2021.3130716>
15. Hsieh, T.-H.; Kiang, J.-F. Comparison of CNN Algorithms on Hyperspectral Image Classification in Agricultural Lands. *Sensors* **2020**, *20*, 1734. <https://doi.org/10.3390/s20061734>
16. Kanthi, M.; Sarma, T.; Chigarpalle, S. Multi-scale 3D-convolutional neural network for hyperspectral image classification. *Indonesian Journal of Electrical Engineering and Computer Science* **2022**, *25*, 307. <https://doi.org/10.11591/ijeecs.v25.i1.pp307-316>
17. Liu, Z.; Wang, Y.; Vaidya, S.; Ruehle, F.; Halverson, J.; Soljacic, M.; Hou, T.Y.; Tegmark, M. KAN: Kolmogorov-Arnold Networks. *arXiv preprint arXiv:2404.19756*, **2024**, 1-50. <https://doi.org/10.48550/arXiv.2404.19756>
18. Vaca-Rubio, C.J.; Blanco, L.; Pereira, R.; Caus, M. Kolmogorov-Arnold Networks (KANs) for Time Series Analysis. *arXiv preprint arXiv:2405.08790*, **2024**, 1-7. <https://doi.org/10.48550/arXiv.2405.08790>
19. Cheon, M. Kolmogorov-Arnold Network for Satellite Image Classification in Remote Sensing. *arXiv preprint arXiv: 2406.00600*, **2024**, 1-10. <https://doi.org/10.48550/arXiv.2406.00600>
20. Wang, Y.; Sun, J.; Bai, J.; Anitescu, C.; Eshaghi, M.S.; Zhuang, X.; Rabczuk, T.; Liu, Y. Kolmogorov Arnold Informed neural network: A physics-informed deep learning framework for solving PDEs based on Kolmogorov Arnold Networks. *arXiv preprint arXiv: 2406.11045*, **2024**, 1-10. <https://doi.org/10.48550/arXiv.2406.11045>
21. Bresson, R.; Nikolentzos, G.; Panagopoulos, G.; Chatzianastasis, M.; Pang, J.; Vazirgiannis, M. KAGNNs: Kolmogorov-Arnold Networks meet Graph Learning. *arXiv preprint arXiv: 2406.18380*, **2024**, 1-15. <https://doi.org/10.48550/arXiv.2406.18380>
22. Hu, W.; Huang, Y.; Wei, L.; Zhang, F.; Li, H. Deep convolutional neural networks for hyperspectral image classification. *Journal of Sensors* **2015**, *2015*, 258619. <https://doi.org/10.1155/2015/258619>
23. Luo, Y.; Zou, J.; Yao, C.; Zhao, X.; Li, T.; Bai, G. HSI-CNN: A Novel Convolution Neural Network for Hyperspectral Image. *Proceedings of International Conference on Audio, Language and Image Processing (ICALIP) 2018*, **2018**, 464-469. <https://doi.org/10.1109/ICALIP.2018.8455251>
24. He, M.; Li, B.; Chen, H. Multi-scale 3D deep convolutional neural network for hyperspectral image classification. *Proceedings of IEEE International Conference on Image Processing (ICIP) 2017*, **2017**, 3904-3908. <https://doi.org/10.1109/ICIP.2017.8297014>
25. Firsov, N.A.; Podlipnov, V.V.; Ivliev, N.A.; Ryskova, D.D.; Pirogov, A.V.; Muzyka, A.A.; Makarov, A.R.; Lobanov, V.; Platonov, V.I.; Babichev, A.N.; Monastyrskiy, V.A.; Olgarenko, V.I.; Nikolaev, D.P.; Skidanov, R.V.; Nikonorov, A.V.; Kazanskiy, N.L.; Soyfer, V.A. Ensembles of spectral-spatial convolutional neural network models for classifying soil types in hyperspectral images. *Computer Optics* **2023**, *47*, 795-805. <https://doi.org/10.18287/2412-6179-CO-1260>
26. Sun, L.; Zhao, G.; Zheng, Y.; Wu, Z. Spectral-spatial feature tokenization transformer for hyperspectral image classification. *IEEE Transactions on Geoscience and Remote Sensing* **2022**, *60*, 5522214. <https://doi.org/10.1109/TGRS.2022.3144158>
27. Li, C.; Liu, X.; Li, W.; Wang, C.; Liu, H.; Yuan, Y. U-KAN Makes Strong Backbone for Medical Image Segmentation and Generation. *arXiv preprint arXiv: 2406.02918*, **2024**, 1-16. <https://doi.org/10.48550/arXiv.2406.02918>
28. Efficient KAN. Available online: <https://github.com/Blealtan/efficient-kan> (accessed on 06 July 2024).
29. PyKAN. Available online: <https://github.com/KindXiaoming/pykan> (accessed on 06 July 2024).
30. ConvKAN. Available online: <https://github.com/StarostinV/convkan> (accessed on 06 July 2024).
31. KA-Conv. Available online: <https://github.com/XiangboGaoBarry/KA-Conv> (accessed on 06 July 2024).
32. Lin, M.; Jing, W.; Di, D.; Chen, G.; Song, H. Multi-Scale U-Shape MLP for Hyperspectral Image Classification. *IEEE Geoscience and Remote Sensing Letters* **2022**, *19*, 6006105. <https://doi.org/10.1109/LGRS.2022.3141547>
33. Jamali, A.; Mahdianpari, M.; Abdul Rahman, A. Hyperspectral image classification using multi-layer perceptron mixer (MLP-MIXER). *Int. Arch. Photogramm. Remote Sens. Spatial Inf. Sci.* **2023**, *XLVIII-4/W6-2022*, 179–182. <https://doi.org/10.5194/isprs-archives-XLVIII-4-W6-2022-179-2023>
34. Meng, Z.; Zhao, F.; Liang, M. SS-MLP: A Novel Spectral-Spatial MLP Architecture for Hyperspectral Image Classification. *Remote Sens.* **2021**, *13*, 4060. <https://doi.org/10.3390/rs13204060>
35. KAN GPT. Available online: <https://github.com/AdityaNG/kan-gpt> (accessed on 06 July 2024).